Journal of Network Intelligence
Taiwan Ubiquitous Information
 ISSN 2414-8105 (Online)
Volume **7**, Number **1**, February **2022**

Vertical Vehicle Dynamics Estimated Inputs with Clouding Road Profiles

Dong-Cherng Lin[1], Trong-The Nguyen[2,3*], Jeng-Shyang Pan[4] , Chang-Der Lee[5]

[1]College of Computer Science and Mathematics,
Fujian University of Technology, Fuzhou 350118, China
[2]Multimedia Communications Lab,
University of Information Technology, VNU-HCM, Vietnam
[3]Vietnam National University, Ho Chi Minh City 700000, Vietnam
[4]College of Computer Science and Engineering,
Shandong University of Science and Technology, Qingdao 266590, China
[5]School of information Engineering, Wuchang University of Technology, Wuchang 430223, China
2046545252@qq.com, ∗thent@uit.edu.vn, jengshyangpan@gmail.com, aeddy8@163.com

Received April 2021, Revision June 2021
(Communicated by ∗thent@uit.edu.vn)

Abstract. *This work suggests two input schemes for determining vertical vehicle dynamics, vertical wheel forces and pitch torques based on Kalman filter (KF). Two different recursive estimators for determining inputs are modeled mathematically by two regression equations: the conventional input estimation (CIE) and adaptive weighting input estimation (AWIE) that are two factors of a tunable fading and adaptive weighting fading, respectively. In numerical simulations, we analyze the current strategy's feasibility and precision with a model driving estimation of wheel loads of a half-car over deterministic. Analyzing and testing datasets of road profiles on the storage cloud are used comparative mapping in the system. The results show that the proposed approach correctly measures the vertical dynamics, and the AWIE task offers greater robust estimation capacity than the vehicle's CIE scheme.*
Keywords: Input estimation; Vehicle vertical dynamics; Recursive least-squares estimator; Cloud computing.

1. **Introduction.** Serious problems for the driver and passengers are caused by the vibration produced due to the road profile's unevenness, which has shown vibration on the ride's comfort [1-2]. Moreover, to interpret the driving environment and be road safety [3], the driving behavior of vehicles and artificial intelligence-based vision is necessary [4], so vertical dynamic estimation plays an important role [5]. In general, there are two methods to obtain inputs, i.e., direct and indirect measurements [6]. The former process is referred to as a scheme that uses force sensors/transducers to receive inputs. The latter approach is referred to as a model-based estimation, input estimation, or force identification, i.e., determining the inputs acting on a system directly from the system responses' measurement. Its displacement or angle employing intermediate force sensors and transducers [7]. So, since we don't use force sensors/transducers but use device responses, estimating road profiles is also input estimation, an overview of the force estimation problem for a linear vibration system [8]. In this way, the designs become their force sensors [9].

A vehicle driving over deterministic profiles (bumps and potholes) or random road profiles, the effect of these road profiles are acting as a base excitation for the system. The methods for estimating the road profiles, based on sliding modes observe [6], on the second-order and third-order sliding modes refer to [8]; based on road profile and vehicle acceleration built a transform function between [10]; an artificial neural network [11]; a wavelet neural network [12] and Kalman filtering (KF) [13] were developed. So, estimating road profiles is also input estimations, when we don't use force sensors and transducers but use system responses.

An approach suggested Kalman inverse filtering using a KF [14] to deconvolve the forces acting from vehicle response measurements at the tire-road interface [15-17]. The basic simple KF [18] with the recursive least-squares estimator has been applied to classify tons of different structures [19]. The simple KF is used with the recursive least-squares estimator (RLSE) [20]. The conventional input estimation (CIE) and the adaptive weighting input estimation (AWIE) schemes are developed [21]. This work applies the CIE and AWIE algorithms for a 2 DOF half-car model. The car model's numerical simulations demonstrate and compare these two methods' accuracy to estimate vertical wheel forces and pitch torques. The current strategy's feasibility and precision with a model driving estimation of wheel loads of a half-car over deterministic are analyzed and the testing dataset of road profiles on storage cloud are used comparative mapping in the system.

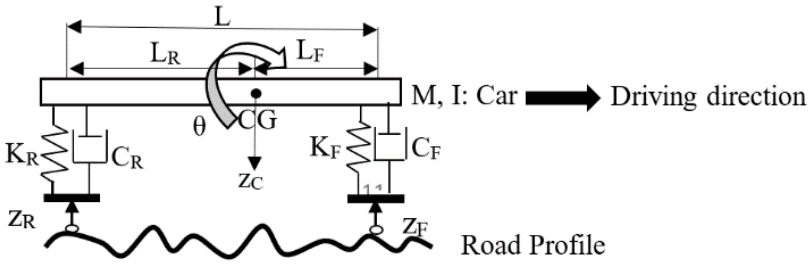

FIGURE 1. Two-dimensional degree-of-freedom half-car model layout

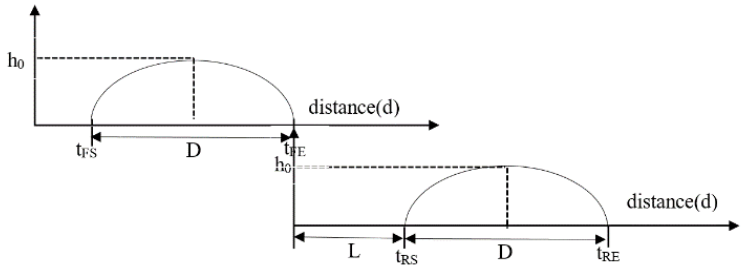

FIGURE 2. The half-car model traveling with constant velocity on a bump that is approximated as a sinusoid, top graph with the front wheel passing, bottom graph, and rear-wheel passing

Contributions of this study are highlighted as follows.

a).Analyzing the current strategy's feasibility and precision with a model driving estimation of wheel loads of a half-car over deterministic. In addition, testing datasets of road profiles on the storage cloud is analyzed for comparative mapping in the system.

b). Modeling mathematically two different recursive estimators for determining inputs with two regression equations: the conventional input estimation (CIE) and adaptive weighting input estimation (AWIE) are two factors of tunable fading and adaptive weighting fading, respectively.

c). Measuring the vertical dynamics, the AWIE task, and comparing robust estimation capacity with the vehicle's CIE scheme.

2. **Related works.** This section reviews the recursive least-squares estimator using Kalman filter, the conventional input estimation, and the adaptive weighting input estimation. Presentations are detailed as follows.

2.1. **Recursive Least-Squares Estimator using Kalman filter.** This section derives the discrete-time state equations of the half-car model subjected to the loads. The input estimation analysis of vertical wheel loads in the model is presented as follows. A half-car model can be used and suited perfectly with a single-track road model [22]. This work, modeling of the system assumptions, the effects of the tires are negligible, and the left side and the right of the car symmetric, shown in Figure 1

Newton's law gives the equation of motions of the half-car model that is expressed as follows.

$$\sum F_z = m\ddot{z} = -F_{S_R} - F_{S_F} - F_{C_R} - F_{C_F} \tag{1}$$

where $F_{S_R} = K_R(z - L_R\theta - z_R), F_{S_F} = K_F(z + L_F\theta - z_F)$, and $F_{C_R} = C_{.R.}(\dot{z} - L_{R.}\dot{\theta} - \dot{z}_R); F_{C_F} = C_F(\dot{z} + L_{F.}\dot{\theta} - \dot{z}_F)$.

and Euler's equation is given as follows:

$$\sum M_{CG} = I\ddot{\theta} = F_{S_R}L_R + F_{S_R}L_R - F_{C_R}L_F - F_{C_F}L_F \tag{2}$$

Two equations (1)and (2) are put into a matrix format as follows:

$$\begin{aligned} &\begin{bmatrix} m & 0 \\ 0 & I \end{bmatrix} \begin{bmatrix} \ddot{z} \\ \ddot{\theta} \end{bmatrix} + \begin{bmatrix} C_F + C_R & C_F L_F - C_R L_R \\ C_F L_F - C_R L_R & C_F {L^2}_F + C_R {L^2}_R \end{bmatrix} \begin{bmatrix} \dot{z} \\ \dot{\theta} \end{bmatrix} \\ &\qquad + \begin{bmatrix} K_F + K_R & K_F L_F - K_R L_R \\ C_F L_F - C_R L_R & K_F {L^2}_F + K_R {L^2}_R \end{bmatrix} \begin{bmatrix} z \\ \theta \end{bmatrix} \\ &\qquad = \begin{bmatrix} C_F\dot{z}_F + C_R\dot{z}_R + K_F z_F + K_R z_R \\ C_F L_F\dot{z}_F - C_R L_R\dot{z}_R + K_F L_F z_F - K_R L_R z_R \end{bmatrix} \end{aligned} \tag{3}$$

where $F_V = C_F\dot{z}_F + C_R\dot{z}_R + K_F z_F + K_R z_R$, and $T_\theta = C_F L_F\dot{z}_F - C_R L_R\dot{z}_R + K_F L_F z_F - K_R L_R z_R$

In the formula: F_V and T_θ are wheel vertical force and pitch torque; $\ddot{z}, \dot{z}, z$ and $\ddot{\theta}, \dot{\theta}, \theta$ are the vertical acceleration, velocity, displacement, angular acceleration, angular velocity, angle of the chassis, respectively; m and I are the mass of the chassis and moment of inertia respectively; $K_F, K_R, C_F, C_R, L_F, L_R$ are spring constants, damping constants in front and rear; L_F, L_R are the length of front and rear to CG, respectively. With the F_V, T_θ, this work determined they by the road profiles estimation. We set the state variables as $X_1 = z, X_2 = z, X_3 = \theta, X_4 = \theta$ when adapting the motion equations with this the state variable notation. A system with the state and measure equations of the continuous-time can be stated as follows.

$$\dot{X}(t) = FX(t) + Gu(t) \tag{4}$$

$$Z(t) = HX(t) \tag{5}$$

where $X(t) = [X_1 X_2 X_3 X_4]^T, u(t) = [F_V T_\theta]$.

and $F = \begin{bmatrix} 0 & 1 & 0 & 0 \\ \frac{-(K_F+K_R)}{m} & \frac{-(C_F+C_R)}{m} & \frac{-(K_F L_F - K_R L_R)}{m} & \frac{-(C_F L_F - C_R L_R)}{m} \\ 0 & 0 & 0 & 1 \\ \frac{-(K_F L_F - K_R L_R)}{I} & \frac{-(C_F L_F - C_R L_R)}{I} & \frac{-(K_F L^2{}_F + K_R L^2{}_R)}{I} & \frac{-(C_F L^2{}_F + C_R L^2{}_R)}{I} \end{bmatrix}$,

$G = \begin{bmatrix} 0 & 0 \\ \frac{1}{m} & 0 \\ 0 & 0 \\ 0 & \frac{1}{I} \end{bmatrix}, H = \begin{bmatrix} 1 & 0 & 0 & 0 \\ 0 & 0 & 1 & 0 \end{bmatrix}$.

With δT length of period times, and based on the inputs of noise process with fictitious [23] [24]. Then Eq. (4) can be expressed as follows.

$$\begin{aligned} X(k+1) &= \Phi X(k) + \Gamma[u(k) + w(k)] \\ X(k) &= [X_1(k) X_2(k) X_3(k) X_4(k)]^T \\ \Phi &= \exp(F \Delta T) \\ \Gamma &= \int_{k\Delta T}^{(k+1)\Delta T} \exp\{F[(k+1)\Delta T - \tau]\} G d\tau \\ w(k) &= [w_1(k) w_2(k)]^T \\ u(t) &= [F_v T_\theta]^T \end{aligned} \tag{6}$$

where $u(k), \Gamma$, and $X(k)$ are the wheel loads, input matrix, and state vector; Γ is the matrix of the state transition, and $w(k)$ is the vector of noise. The mean is assumed as zero and variance white with $Ew(k)wT(j) = Q\Gamma_{kj}$, in which Γ_{kj} expresses as the delta function. The statistical measurement noise equation of Eq. (5) can be expressed as follows.

$$\begin{aligned} Z(k) &= HX(k) + v(k) \\ Z(k) &= [Z_1(k) Z_2(k)]^T \\ v(k) &= [v_1(k) v_2(k)]^T \end{aligned} \tag{7}$$

where H and $Z(k)$ are the measured variable matrix, and observed vector, respectively; $v(k)$ is the vector of measured noise, where $v(k)$ is supposed as zero with white noise its means; and its variance is set as $Ev(k)v^T(j) = R\Gamma kj$, and $R = \theta^2$, where θ is the standard deviation of the measured noise. The magnitudes of the F_V and T_θ, are wheel vertical force, and pitch torque can be estimated from the car model responses.

2.2. **Conventional input estimation.** Conventional input estimation (CIE), the discrete-time state equations for the half-car model subject, is taken for vertically loading as in the previous section. The F_V magnitudes, T_θ, are wheel vertical force and pitch torque can be estimated from the system responses by the proposed input estimation schemes. The CIE, a simple KF, and a recursive least-squares algorithm can be found in [21]. The simple KF equations are:

$$\bar{X}(\frac{k}{k+1}) = \Phi \bar{X} \cdot (\frac{k-1}{k-1}) \tag{8}$$

$$P(\frac{k}{k-1}) = \Phi P(\frac{k-1}{k-1}) \Phi^T + \Gamma Q \Gamma^T \tag{9}$$

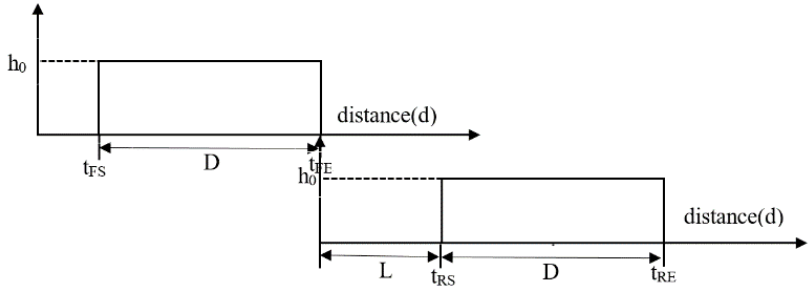

FIGURE 3. The half-car model traveling with constant velocity on a rectangular cleat, top graph: front wheel passing, bottom graph: rear wheel passing

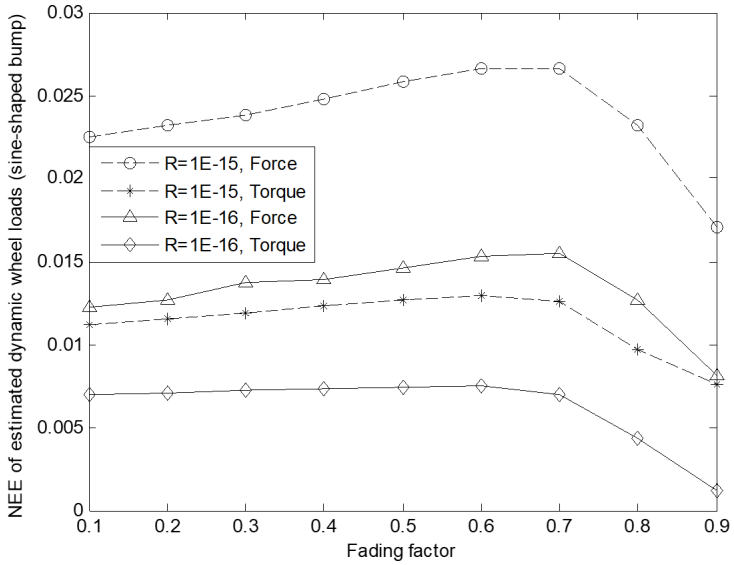

FIGURE 4. The NEE of the estimated dynamic loads vs. fading factors at $R = 1E-15$ ($i.e., 1 \times 10^{-15}$) to $1E-16$ with $Q = 1E2$ for the driving half-car model on a sine-shaped bump with v =30km/hr

$$S(k) = HP(\frac{k}{k-1})H^T + R \tag{10}$$

$$K_a(k) = P(\frac{k}{k-1})H^T S^{-1}(k) \tag{11}$$

$$P(\frac{k}{k}) = [I - K_a(k) \centerdot H] \centerdot P(\frac{k}{k-1}) \tag{12}$$

$$\bar{Z}(k) = Z(k) - H\bar{X}(\frac{k}{k-1}) \tag{13}$$

$$\bar{X}(\frac{k}{k}) = \bar{X}(\frac{k}{k-1}) + K_a(k)\bar{Z}(k) \tag{14}$$

The equations for a recursive least-squares algorithm with a tuning fading factor are:

$$B_s(k) = H[\Phi M_s(k-1) + I]\Gamma \tag{15}$$

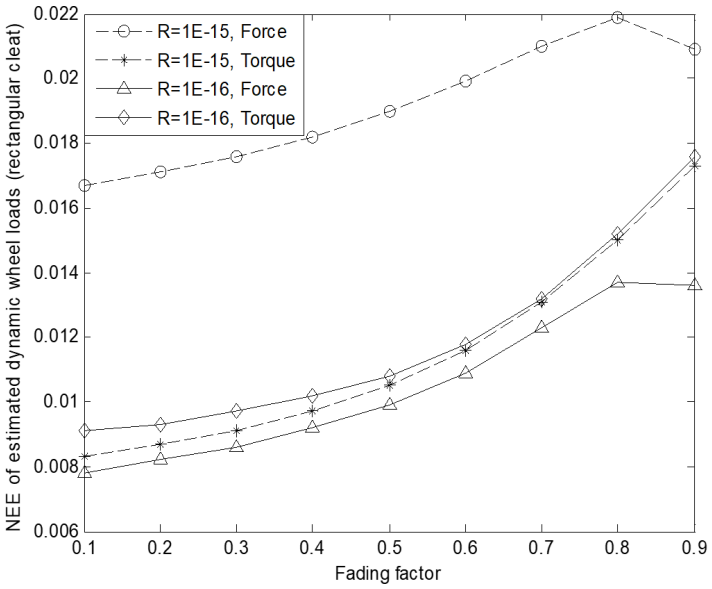

FIGURE 5. The NEE of the estimated dynamic loads vs. fading factors at $R = 1E-15$ to $1E-16$ with $Q = 1E2$ for the driving half-car model on a rectangular cleat with v =30km/hr

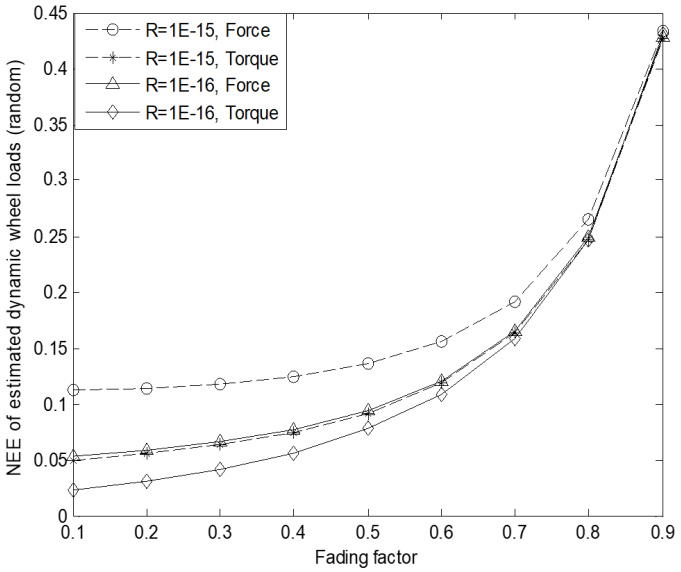

FIGURE 6. The NEE of the estimated dynamic loads vs. fading factors at R with $1E-15$ to $1E-16$ with $Q = 1E2$ for the driving half-car model on a random road with v =30km/hr

$$M_s(k) = [I - K_a(k)H][\Phi M_s(k-1) + I] \tag{16}$$

$$K_b(k) = f_{tr}^{-1} P_b(k-1) B_S^T(k) [B_s(k) f_{tr}^{-1} P_b(k-1) B_S^T(k) + S(k)]^{-1} \tag{17}$$

$$P_b(k) = [I - K_b(k) B_s(k)] f_{tr}^{-1} P_b(k-1) \tag{18}$$

$$\hat{u}_{CIE}(k) = \hat{u}_{CIE}(k+1) + K_b(k)[\bar{Z}(k) - B_s(k)\hat{u}_{CIE}(k-1)] \tag{19}$$

In the formular, $S(k)$ and $\bar{Z}(k)$ are the innovation covariances and $K_b(k)$ is Kalman gain that are obtained from the Kalman filter; P_b is the error covariance of the estimated input vector, f_{tr} represents the fading factor, and $B_s(k)$ and $M_s(k)$ are sensitivity matrices, $K_b(k)$, $\hat{u}_{CIE}(k)$, and $P_b(k)$ are the correction gain for the updating, the error covariances of the estimated input vector; where $\hat{u}_{CIE}(k)$ is a vertical loads vector. Therefore, the vertical wheel forces and pitch torques can be estimated using the CIE approach is as follows:

• Identify the state-variable model given by Eqs. (1) – (5), the discretized state-variable model, as described by Eqs. (6) and (7), and measure the dynamic response data of the half-car model system.

• Simple KF equations are used as in the Eqs. (8) – (14) to obtain the innovation covariance $S(k)$, innovation $\bar{Z}(k)$, and KF gains $K_a(k)$.

• Recursive least-squares algorithm is applied with a tunable fading factor, Eqs. (15) – (19), to estimate the dynamic wheel loads $\hat{u}_{CIE}(k)$.

The proposed algorithms use the fading factor ftr to balance the fast adaptive capacity and the lack of precision of the estimation. here.

2.3. **Adaptive weighting input estimation.** The adaptive weighting input estimation (AWIE) is the main objective of creating a robust fading factor in the adaptively modified algorithm according to the residual innovation sequence of the simple KF at each point. The thorough derivation of the fading element of adaptive weighting refers to the literature [21] options. Finally, Eqs. (20) – (22) are expressed as follows.

$$K_b(k) = ftr_{aw}^{-1} P_b(k-1)^{B_S^T}(k)[B_s(k) ftr_{aw}^{-1} P_b(k-1)^{B_S^T}(k) + S(k)]^{-1} \tag{20}$$

where $ftr_{aw}(k) = \begin{cases} 1 & |\bar{z}(k)| \le \sigma \\ \sigma/|\bar{z}(k)| & |\bar{z}(k)| > \sigma \end{cases}$

$$P_b(k) = [I - K_b(k)B_s(k)] ftr_{aw}^{-1} P_b(k-1) \tag{21}$$

$$\hat{u}_{AWIE}(k) = \hat{u}_{AWIE}(k-1) + K_b(k)[\bar{Z}(k) - B_s(k)\hat{u}_{AWIE}(k-1)] \tag{22}$$

The estimating vertical dynamics are calculated scheme mathematically as a procedure by applying the AWIE scheme is given in detail below. The CIE scheme is used to identify two steps first. Then, the recursive least-squares strategy is applied with an adaptive weighting fading factor that refers to Eqs. (15), (16), and (20) – (22), to estimate vertical wheel forces and pitch torques $\hat{u}_{AWIE}(k-1)$.

3. Experimental Results.

3.1. **Scenario environmental setting experiment.** A half-car model is driven with different constant velocities, e.g., 30, 60, 90km/hr, over three types of road profile, e.g., the random road, sine-shaped bump, and rectangular cleat profiles. In the first numerical experiment, the car is driven over the sine-shaped bump, the vertical motion of the axles z_F (front wheel) and z_R(rear wheel). Figure 2 shows a half-car model scenario traveling with constant velocity on a bump approximated as a sinusoid, top graph with the front wheel passing, bottom graph, and rear-wheel passing.

$$Z_F = \begin{cases} 0 & if\, t < t_{FS} \\ h_0 \sin(w_f t), w_f = \frac{\pi v}{D}, & if\, t_{FS} \le t \le t_{FE} \\ 0 & if\, t > t_{FE} \end{cases} \tag{23}$$

TABLE 1. The parameters of the driving half-car model.

Parameters	Values	Parameters	Values	Parameters	Values
m	2000 (kg)	C_F	500 (N·s/m)	L	2 (m)
I	600 (kg-m^2)	C_R	500 (N·s/m)	h_0	0.1 (m)
K_F	5000 (N/m)	L_F	0.8 (m)	D	1 (m)
K_R	5000 (N/m)	L_R	1.2 (m)		

$$Z_R = \begin{cases} 0 & if\, t < t_{RS} \\ h_0 \sin(w_f t), w_f = \frac{\pi v}{D}, & if\, t_{RS} \le t \le t_{RE} \\ 0 & if\, t > t_{RE} \end{cases} \tag{24}$$

where v and w_f are the car velocity and angular frequency respectively; h_0 and d are the height of the bump, and horizontal coordinate; D and L are the length of the bump and distance between the front and rear wheel, t_{FS} and t_{FE} are the front wheels starting time and front-wheel ending time; t_{RS} and t_{RE} are the rear wheels starting time and rear-wheel ending time, respectively.

The estimated error (NEE) in Eq. (28) is termed the normalized one to get the optimal estimatition with NEE of dynamic wheel loads; the tune the fading factor f_{tr} in Q is assumed one level to set as $1E2$, two levels of measurement noise σ is set to $1E-7.5$ and $1E-8$, respectively. Table 1 lists the setting parameters for the half-car model.

Using Eqs. (23a) and (23b) in Eqs. (3a) and (3b), we obtained the wheel vertical force and pitch torque as follows:

$$\begin{aligned} F_{v-\sin} = {} & h_0(1-U_{tp1})[K_F \sin(wft) + C_{Rwf}\cos(wft)] \\ & + h_0(U_{tL}-U_{tP1})[K_R \sin(wft) + C_{Rwf}\cos(wft)] \end{aligned} \tag{25}$$

$$\begin{aligned} F_{\theta-\sin} = {} & h_0 L_F(1-U_{tp1})[K_F \sin(wft) + C_{Fwf}\cos(wft)] - h_0 L_R(U_{tL} \\ & - U_{tP1})[K_R \sin(wft) + C_{Rwf}\cos(wft)] \end{aligned} \tag{26}$$

where

$$U_{tp1} = \begin{cases} 0, & if\, t \le t_{FE} \\ 1, & if\, t > t_{FE} \end{cases}; U_{tL=} \begin{cases} 0, & if\, t \le t_{RS} \\ 1, & if\, t > t_{RS} \end{cases}; U_{tp2=} \begin{cases} 0, & if\, t \le t_{RE} \\ 1, & if\, t > t_{RE} \end{cases}$$

In the secondary numerical experiment, the car is driven over rectangular cleat. Figure 3 illustrates a half-car model scenario of traveling with constant velocity on a rectangular cleat, top graph: front wheel passing, bottom graph: rear wheel passing. Simplifying the wheel vertical force and pitch torque in Eqs. (3a) and (3b), can be written as follows.

$$F_{v-rect} = h_0(1-U_{tp1})K_F + h_0(U_{tL}-U_{tp1})K_R \tag{27}$$

$$F_{\theta-rect} = h_0 L_F(1-U_{tp1})K_F - h_0 L_R(U_{tL}-U_{tp1})K_R \tag{28}$$

where

$$U_{tp1} = \begin{cases} 0, & if\, t \le t_{FE} \\ 1, & if\, t > t_{FE} \end{cases}; U_{tL=} \begin{cases} 0, & if\, t \le t_{RS} \\ 1, & if\, t > t_{RS} \end{cases}; U_{tp2=} \begin{cases} 0, & if\, t \le t_{RE} \\ 1, & if\, t > t_{RE} \end{cases}$$

In the third numerical experiment, the car is driven over ISO-8608 random road profile [25] at this period. Simplifying the wheel vertical force and pitch torque in Eqs. (3a) and (3b), can be written as follows:

$$F_{v-rand} = K_F \times z_R(s) + K_R \times z_R(s) \tag{29}$$

$$F_{\theta-rand} = K_F \times L_F \times z_R(s) - K_R \times L_R \times z_R(s) \tag{30}$$

where $z_R(s) = \sum_{i=1}^{N} A_i \sin(\Omega_i s - \Psi_i)$

$$A_i = \sqrt{2\Phi(\Omega_i)\Delta\Omega}, i = 1 \sim N \tag{31}$$

where Ω_i : wavenumbers are chosen to lie at N equal interval $\Delta\Omega$, Ψ_i : phase angles The simulation parameters consist of a sampling interval of ΔT is set to 0.001 sec, and a final time t_f is set to 1.2 sec. The exact and loads estimations validate the proposed approach with its error metric as defined expression as follows.

$$Error = \frac{\sqrt{\sum_{k=1}^{n} u_{Exact}^2(k)} - \sqrt{\sum_{k=1}^{n} \hat{u}_{Est}^2(k)}}{\sum_{k=1}^{n} u_{Exact}^2(k)} \times 100\% \tag{32}$$

3.2. **Several obtained results.** Several obtained results are represented as follows. (1) Dynamic wheel load types are estimated in the half-car model with a 30km/hr velocity crossing the three different road profile types. Figures 10 to 12 depict the obtained estimation results from the AWIE and CIE approaches. Figures 10(a), 10(b), 11(a), 11(b) and 12(a), 12(b) displays the experimental results with $f_{tr} = 0.1$, Figures 10(c), 10(d), 11(c), 11(d) and 12(c), 12(d) the experimental results $f_{tr} = 0.9$, for the wheel vertical forces and pitch torques, respectively.

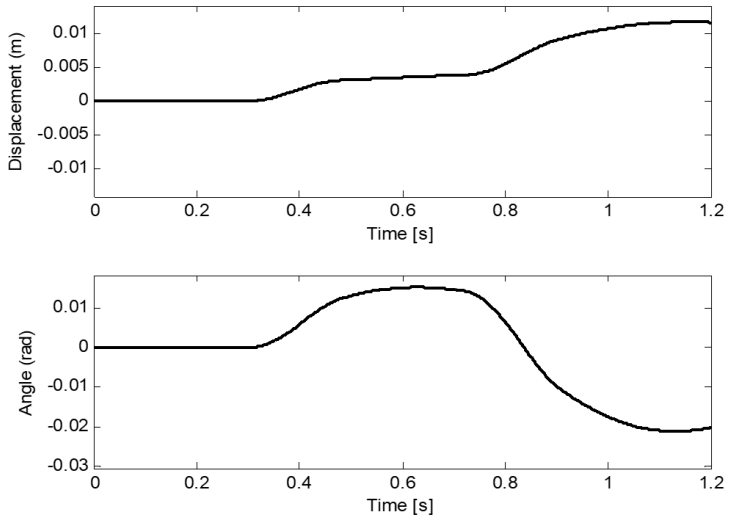

FIGURE 7. The simulated output displacement and angle for the driving half-car model on sine-shaped bump with setting $v = 30$km/hr, $\sigma = 1E-8$, $Q = 1E2$

Figure 12(d). The pitch torques of the obtained estimation for the driving half-car model on the random road profile with $v = 30km/hr$: (a) AWIE scheme; (b) CIE scheme ($f_{tr} = 0.9$), respectively. (2) Table 2 summarizes the NEEs of the dynamic wheel load types for the half-car model with a velocity of 30km/hr in the three road profiles. The

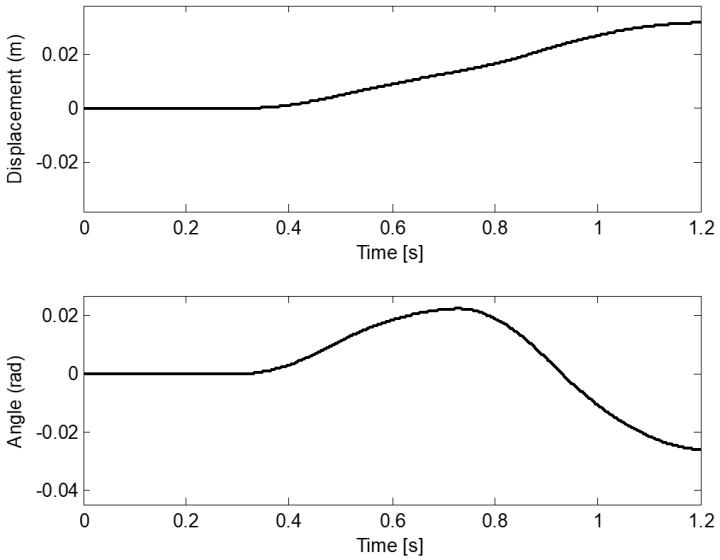

FIGURE 8. The obtained simulation output displacement and angle for the driving half-car model n the rectangular-cleat with setting $v = 30$km/hr, $\sigma = 1E-8$, $Q = 1E2$

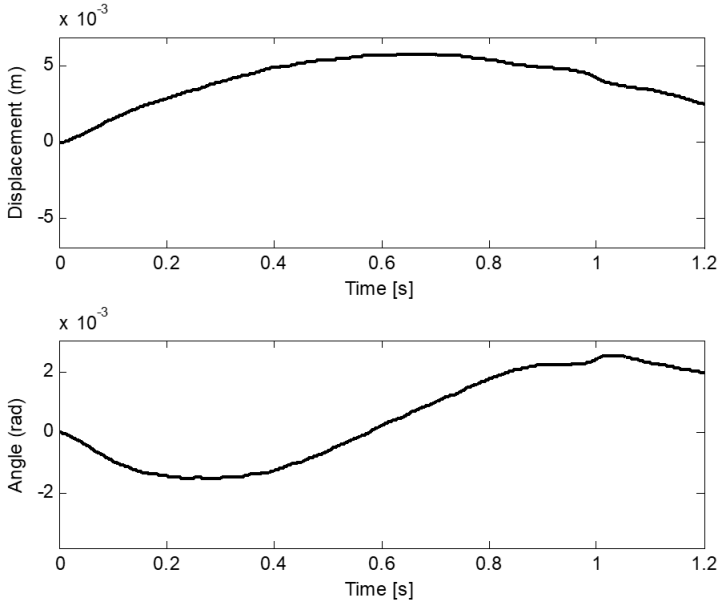

FIGURE 9. The simulated output displacement and angle for the driving half-car model on the random-road with setting $v = 30$km/hr,$\theta = 1E-8(i.e., 1 \times 10^{-8}), Q = 1E2(i.e., 1 \times 10^{2})$.

NEE of wheel loads type is within 4.93%for the AWIE method and within 5.33% for the CIE method with $f_{tr} = 0.1$. The NEE of wheel load type in the half-car model crossing sine-shaped bump and rectangular cleat are within 1.76%, crossing random road profile are within 43.03% for the CIE method with $f_{tr} = 0.9$.

In work, the initial conditions for the approaches are given by: the state vector is a 4-by-1 zero matrix and the filter's error covariance matrix is a 4-by-4 diagonal matrix of 1E10 for the simple KF, the error covariance is a 2-by-2 diagonal matrix of 1E8, the sensitivity matrix is a 4-by-4 zero matrix and wheel loads is a 2-by-1 as zero matrices with

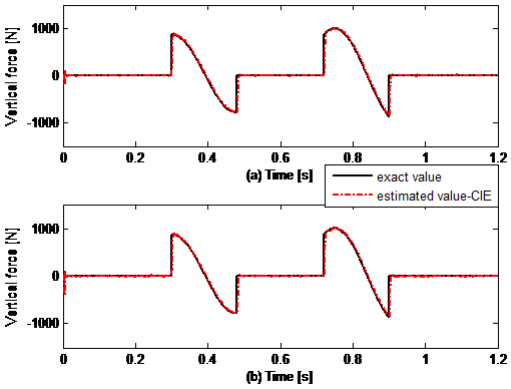

(A) Wheel vertical forces estimation

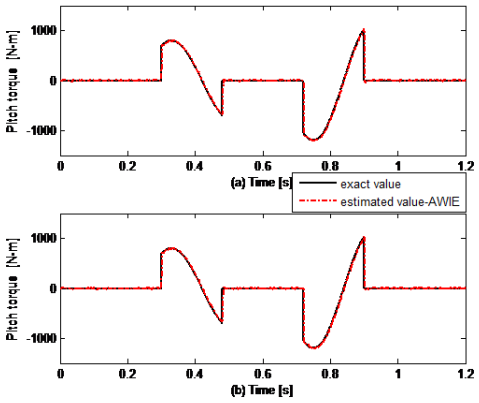

(B) Pitch torques obtained estimation

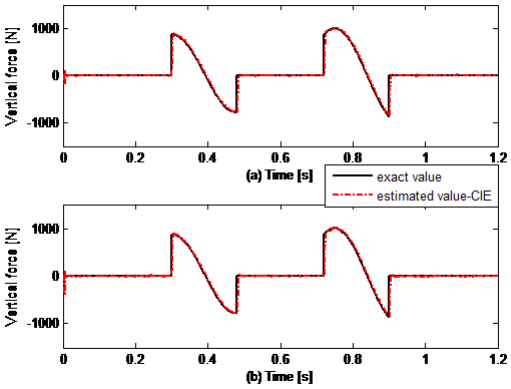

(C) Wheel vertical forces estimation

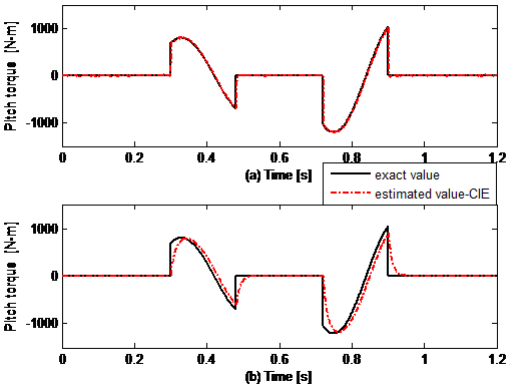

(D) Pitch torques of the obtained estimation

FIGURE 10. Wheel vertical forces and Pitch torques of the obtained estimations for the driving half-car model on the sine-shaped bump with setting v =30km/hr over (a) AWIE scheme and (b) CIE scheme (f_{tr} = 0.9), respectively

TABLE 2. The NEE of the three estimated dynamic wheel load types for the driving half-car model over three road profiles with a velocity of 30km/hr

Types of road profiles	Wheel load type	CIE (*ftr* = 0.1)	CIE (ftr = 0.9)	AWIE
Sine-shaped bump	Vertical force	1.22%	0.81%	4.91%
	Pitch torque	0.70%	1.24%	1.42%
Rectangular cleat	Vertical force	0.78%	1.36%	0.61%
	Pitch torque	0.91%	1.76%	0.63%
Random	Vertical force	5.33%	42.85%	4.93%
	Pitch torque	2.24%	43.03%	2.13%

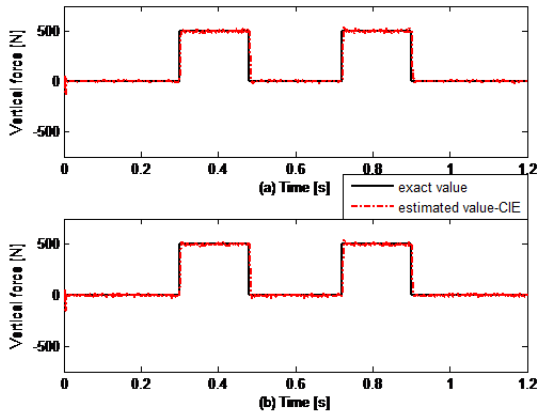

(A) Wheel vertical forces estimation

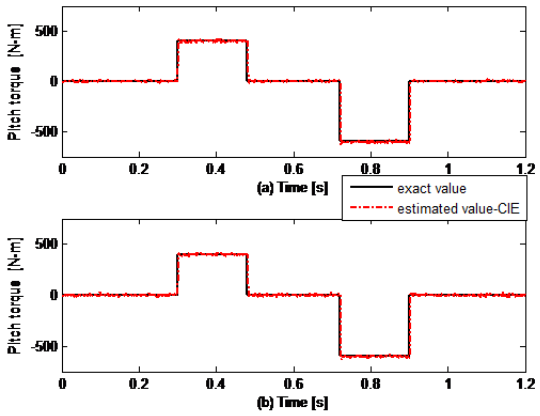

(B) Pitch torques obtained estimation

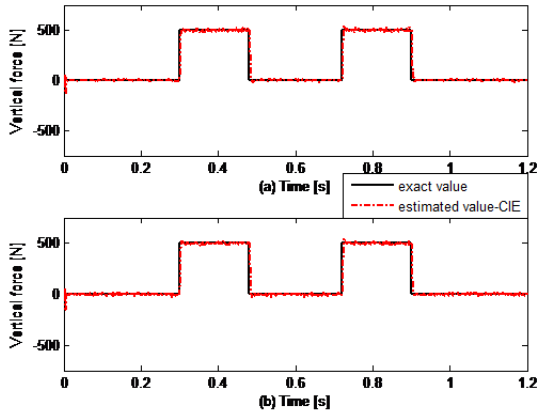

(C) Wheel vertical forces estimation

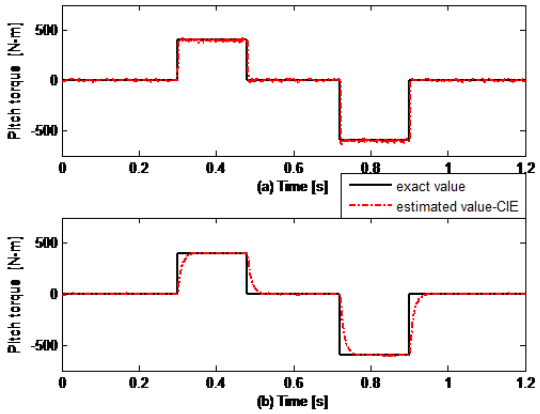

(D) Pitch torques of the obtained estimation

FIGURE 11. Wheel vertical forces and the pitch torques of the obtained estimation for the driving half-car model on the rectangular cleat with setting $v = 30$km/hr: (a) AWIE scheme and (b) CIE scheme ($f_{tr} = 0.9$), respectively

applying the least-squares algorithms. The obtained value of the NEE with three dynamic wheel load types indicates that the half-car model-driven over the sine-shaped bump and rectangular cleat significantly less than the random road profile when $0.1 \leq ftr \leq 0.9$. Figures 4 to 6 illustrate the NEE's comparison of the estimated dynamic loads with different fading factors for the driving half-car model over the varieties roads.

Additionally, the estimation results for the wheel vertical force and pitch torque in the car driven over the three different road profile types are good, and all NEE values are within 5.33% at $\theta = 1E-8$ with $Q = 1E2$, when $f_{tr} = 0.1$ in CIE, and AWIE approaches (in Table 2). The fading factor f_{tr} discards old data by weighting data according to the occurred data time. The measurement noise covariance must have been increased in comparison with the previous measurements. e.g., the estimated optimization method [26]. Therefore, in numerical experiments, $f_{tr} = 0.1$ is used to compare the AWIE, and CIE approaches' efficiency and robustness with $\theta = 1E-8$ with $Q = 1E2$. As well as demonstrate the accuracy of the half-car model system's proposed methods, the vertical wheel forces and pitch torques are estimated with output responses, displacement, and angle (Figs. 7-9).

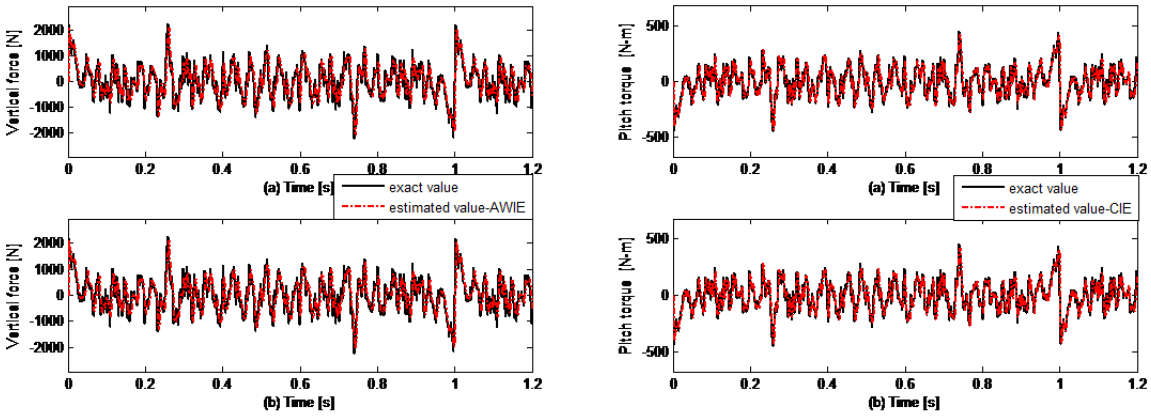

(A) Wheel vertical forces estimation (B) Pitch torques obtained estimation

FIGURE 12. Wheel vertical forces and the pitch torques of the obtained estimation for the driving half-car model on the rectangular cleat with setting v = 30km/hr: (a) AWIE scheme and (b) CIE scheme (f_{tr} = 0.9), respectively

TABLE 3. The NEE of the three estimated dynamic wheel load types for the driving half-car model over three road profiles with different constant velocity (km/hr)

Types of road profiles	Wheel load type	CIE (v=30)	AWIE (v=30)	CIE (v=60)	AWIE (v=60)	CIE (v=90)	AWIE (v=90)
Sine-shaped bump	Vertical force	1.22%	4.91%	0.74%	0.57%	1.22%	1.07%
	Pitch torque	0.70%	1.42%	0.30%	0.43%	0.71%	0.67%
Rectangular cleat	Vertical force	0.78%	0.61%	1.85%	1.56%	2.93%	1.84%
	Pitch torque	0.91%	0.63%	1.49%	1.11%	2.38%	2.50%
Random	Vertical force	5.33%	4.93%	5.23%	4.94%	5.28%	4.84%
	Pitch torque	2.24%	2.13%	2.30%	1.85%	1.75%	1.71%

(3) Table 3 summarize the NEEs of the dynamic wheel load types for the half-car model in the three road profiles with different constant velocity (30, 60, 90km/hr). The NEE of wheel load type is within 5.33% for the CIE method with f_{tr} = 0.1 and the AWIE method.

(4) Dynamic wheel load types are estimated in the half-car model with a velocity of 90km/hr crossing three different road profile types. Figures 13– 15 show estimation results for the AWIE and CIE (with $f_{tr} = 0.1$) approaches, the simulation results for the vertical wheel forces and pitch torques, respectively.

(5) An oscillating motion from front to rear is referred to as pitching that pitches if the rough road's wavelengths are such that the front and rear's vertical movements are in opposition process. This implies if, as the rear goes up on a bump or vice versa, the front axle drops into a depression. Figures 10(b), 10(d), 11(b), 11(d), 13(b), and 14(b) show the pitch torques of the obtained estimation for the driving half-car model on the rectangular cleat with parameter setting variety values.

3.3. **Experimental discussions.** Some achieved results reveal that the proposed scheme correction are listed as follows.

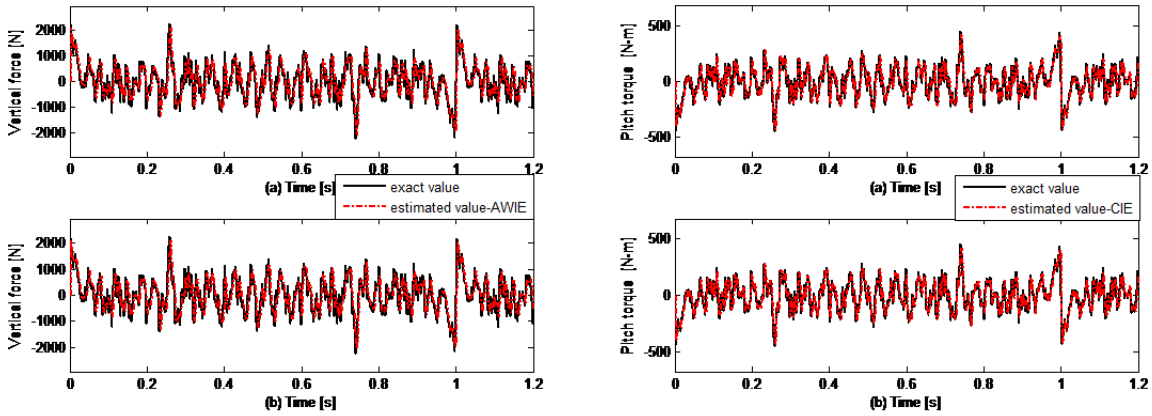

(A) Wheel vertical forces estimation (B) Pitch torques obtained estimation

FIGURE 13. Wheel vertical forces and the pitch torques of the obtained estimation for the driving half-car model on the sine-shaped bump with $v = 90km/hr$: (a) AWIE scheme; (b) CIE scheme ($f_{tr} = 0.1$), respectively.

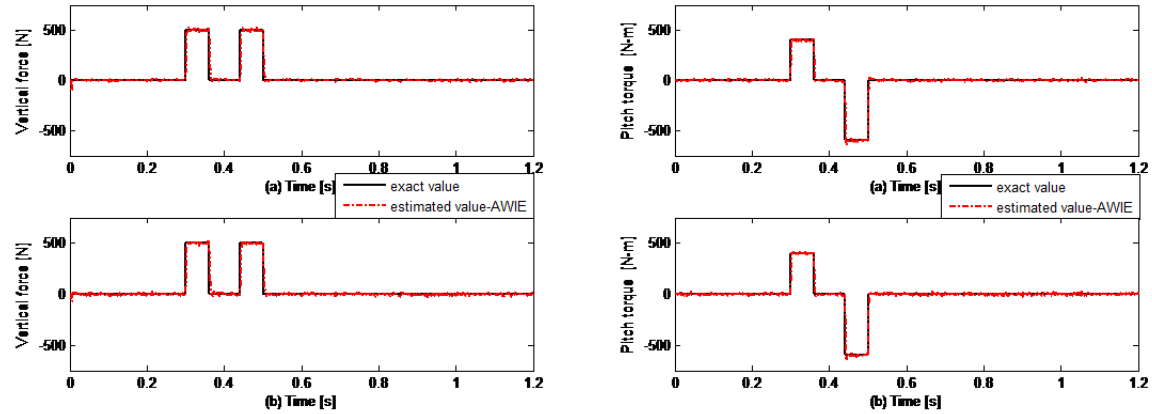

(A) Wheel vertical forces estimation (B) Pitch torques obtained estimation

FIGURE 14. The vertical wheel forces and pitch torques of the obtained estimation for the driving half-car model on the rectangular cleat with $v = 90km/hr$: (a) AWIE scheme; (b) CIE scheme ($f_{tr} = 0.1$), respectively

(1) The proposed methods had substantial errors in the initial estimate, but after a few time step, the estimated rapidly converge to the exact values as shown in Figures 10(a), 10(c), 11(a), 11(c), 13(a) and 14(a), these simulation results reveal that the proposed scheme can correct the error in the initial estimate by using tremendous values of the filter's error covariances and the error covariances.

(2) For comparing estimated results with $\sigma = 1E - 7.5$ and $1E - 8$, investigated that the determined results for $\sigma = 1E - 7.5$ have larger NEEs than those for $\sigma = 1E - 8$. Figures 4 to 6 show the NEE of the estimated dynamic loads vs. different fading factors. The estimated accuracy is reduced, this is because of considerable measurement noise. For $\sigma = 1E - 8$, a high precision measurement sensor is needed. (3) In terms of the energy content, the dynamic wheel loads estimation for the driving half-car model over three different road profile types with $v = 30km/hr$, (a) the NEEs of vertical wheel forces are 4.91%, 0.61%, and 4.93%; pitch torques are 1.42%, 0.63% and 2.13% using the AWIE

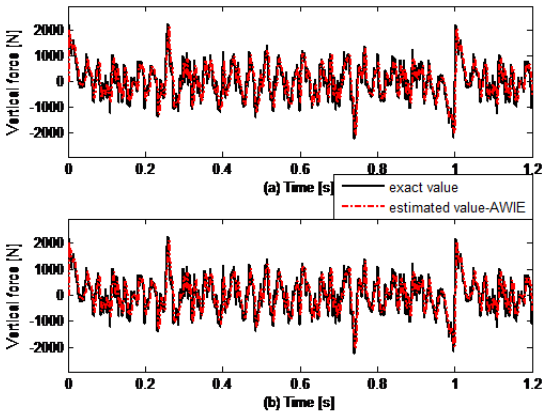

(A) The vertical wheel forces of the obtained estimation

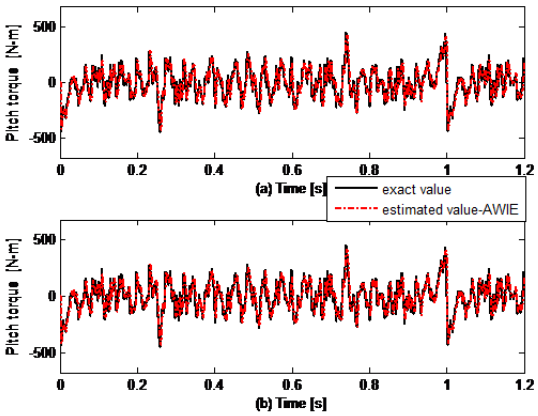

(B) The pitch torques of the obtained estimation

FIGURE 15. The vertical wheel forces and the pitch torques of the obtained estimation for the driving half-car model on random road profile with setting $v = 90$km/hr: (a) AWIE scheme; (b) CIE scheme ($f_{tr} = 0.1$), respectively

method, (b) the NEEs of vertical wheel forces are 1.12%, 0.78%, and 5.33%; pitch torques are 0.70%, 0.91% and 2.24% using the CIE method with $f_{tr} = 0.1$, respectively. Table 2 lists the NEE of the three estimated dynamic wheel load types for the driving half-car model over three road profiles with a velocity of 30km/hr. There aren't change abruptly for estimated loads in the rectangular cleat shown as in Figures 11, and 14; the loads' estimated error results from less than estimated loads in sine-shaped bump and random road profile as shown in Figures 4 to 6. Additionally, the calculated results pitch torques better than vertical forces using CIE and AWIE approaches.

The dynamic wheel loads estimation results for the half-car model-driven over three different road profile types with car velocity $v = 30, 60, 90 km/hr$ are good, and NEE values are within 5.33%, when $f_{tr} = 0.1$ in CIE and AWIE approaches. Table 3 depicts the NEE of the three estimated dynamic wheel load types for the driving half-car model over three road profiles with different constant velocities (km/hr). Additionally, the estimated results pitch torques better than vertical forces using CIE and AWIE approaches.

(4) The AWIE and CIE schemes' obtained estimation results with f_{tr} are set to 0.1 that are excellent agreements with the exam vertical wheel forces' exact values and pitch torques in the cosine-shaped bump, rectangular cleat, and random road profile types when car velocity $v = 30 km/hr$. Figures 10(a), (b), 11(a), (b), and 12(a), (b)) show the vertical wheel forces of the obtained estimation for the driving half-car model on the rectangular cleat with different setting parameters. Figures 13 to 15 show the obtained results with parameter setting v is set to 90km/hr. Nevertheless, in three different road profiles, the measurement results of the CIE method with $f_{tr} = 0.9$ vary substantially from the exact values of the vertical wheel forces and pitch torques at vehicle velocity as shown in Figures 10(c), (d), 11(c), (d), and 12(c), (d). Therefore, as the inference is drawn in Figures 10(a), (b), 11(a), (b), and 12(a), (b), as well as, the same simulation results are obtained for the velocity change Figures 13 – 15, the adaptive weighting fading factor has adequate and robust estimation performance.

(5) Pitching oscillating movement can occur by the vehicle wheel based on a previous multiple half-car models over the road surface uneven wavelength [27]. The work, wheelbase of the half-car model, is set 2m, a wavelength of the cosine-shaped bump and

rectangular cleat are set to $1m$, and the car driven over the road profiles. So, there are pitching appearances in Figures 10(b), 10(d), 11(b), 11(d), 13(b), and 14(b).

(6) The aim of vertical dynamics is to tuning body suspension and damping to guarantee good ride comfort, respectively minimal stress of the load at sufficient safety. According to the simulation estimated results, these body suspension spring force and damping force in Eqs. (1a), (1b) can also be assessed using the two inverse methods. After all, they can estimate the input (road profile) from the system output in inverse.

4. **Conclusion.** This paper analyzed the current strategy's feasibility and precision with a model driving estimation of wheel loads of a half-car over deterministic. The half-car model's vertical dynamics are identified using the two estimated input methods, e.g., the conventional input estimation (CIE) and adaptive weighting input estimation (AWIE) schemes. The instance scenarios verify the accuracy of the wheel vertical forces' estimation results and pitch torques for the CIE scheme with a fading factor, e.g., a symbol factor of f_{tr} is set 0.1 and the AWIE scheme. The tracking of the random vertical dynamics can offer the perfect performance of the methods. Moreover, a comparison of efficiency and robustness results indicates that the AWIE approach has superior robust estimation capability than the half-car model system's CIE scheme. Referring to the dataset of road profiles on storage cloud is used comparative mapping in the system. The experimental results also show that the proposed method correctly measures the vehicle's vertical dynamics compared with the literature as similar as in [21]. Future work will apply to various fields [28-33], e. g., vibration and noise guidance.

REFERENCES

[1] S.-H. Chen, J.-S. Pan, K. Lu, and H. Xu, Driving behavior analysis of multiple information fusion based on adaboost, *in Genetic and Evolutionary Computing, Springer*, 2015, pp. 277–285.

[2] V. Rouillard, M. A. Sek, and T. Perry, Analysis and simulation of road profiles, *Journal of Transportation Engineering,* vol. 122, no. 3, pp. 241–245, 1996.

[3] J.-S. Pan, K. Lu, S.-H. Chen, and L. Yan, Driving Behavior Analysis of Multiple Information Fusion Based on SVM, *in International Conference on Industrial, Engineering and Other Applications of Applied Intelligent Systemsin, 2014*, pp. 60–69.

[4] S.-H. Chen, J.-S. Pan, and K. Lu, Driving behavior analysis based on vehicle OBD information and adaboost algorithms, *in Proceedings of the international multiconference of engineers and computer scientists,* 2015, vol. 1, pp. 18–20.

[5] Y. Nakamura, A method for dynamic characteristics estimation of subsurface using microtremor on the ground surface, *Railway Technical Research Institute, Quarterly Reports*, vol. 30, no. 1, pp. 25-33, 1989.

[6] H. Imine, Y. Delanne, and N. K. M'sirdi, Road profile inputs for evaluation of the loads on the wheels, *International Journal of Vehicle Mechanics and Mobility,* vol. 43, no. (sup) 1, pp. 359–369, 2005.

[7] H. Imine, Y. Delanne, and N. K. M'sirdi, Road profile input estimation in vehicle dynamics simulation, *International Journal of Vehicle Mechanics and Mobility*, vol. 44, no. 4, pp. 285–303, 2006.

[8] H. Imine and L. Fridman, Road profile estimation in heavy vehicle dynamics simulation, *International Journal of Vehicle Design*, vol. 47, no. 1–4, pp. 234–249, 2008.

[9] K. K. Stevens, Force identification problems an overview, *in Proceedings of the 1987 SEM Spring Conference on Experimental Mechanics, Houston, TX, USA,* 1987, pp. 838–844.

[10] S. Eben Li, K. Li, and J. Wang, Economy-oriented vehicle adaptive cruise control with coordinating multiple objectives function, *International Journal of Vehicle Mechanics and Mobility*, vol. 51, no. 1, pp. 1–17, 2013.

[11] M. Yousefzadeh, S. Azadi, and A. Soltani, Road profile estimation using neural network algorithm, *Journal of Mechanical Science and Technology* , vol. 24, no. 3, pp. 743–754, 2010.

[12] A. Solhmirzaei, S. Azadi, and R. Kazemi, Road profile estimation using wavelet neural network and 7-DOF vehicle dynamic systems, *Journal of Mechanical Science and Technology*, vol. 26, no. 10, pp. 3029–3036, 2012.

[13] D. Simon, Kalman filtering, *Embed. Syst. Program.*, vol. 14, no. 6, pp. 72–79, 2001.
[14] R. E. Kalman, A new approach to linear filtering and prediction problems, *Transactions of the ASME–Journal of Basic Engineering*, vol. 82 (Series D), pp. 35-45, 1960.
[15] L. R. Ray, Nonlinear state and tire force estimation for advanced vehicle control, *IEEE Transactions on Control Systems Technology,* vol. 3, no. 1, pp. 117–124, 1995.
[16] L. R. Ray, Nonlinear tire force estimation and road friction identification: Simulation and experiments, *Automatica,* vol. 33, no. 10, pp. 1819–1833, 1997.
[17] K. Huh and J. Kim, Active steering control based on the estimated tire forces, *Journal of Dynamic Systems, Measurement, and Control*, vol. 123, no. 3, pp. 505–511, 2001.
[18] Y. T. Chan, A. G. C. Hu, and J. B. Plant, A Kalman filter based tracking scheme with input estimation, *IEEE Transactions on Aerospace and Electronic Systems*, no. 2, pp. 237–244, 1979.
[19] C.-K. Ma and D.-C. Lin, Input forces estimation of a cantilever beam,*Inverse Problems in Science and Engineering*, vol. 8, no. 6, pp. 511–528, 2000.
[20] S. Wen, H. Qi, Y.-T. Ren, J.-P. Sun, and L.-M. Ruan, Solution of inverse radiation-conduction problems using a Kalman filter coupled with the recursive least–square estimator, *International Journal of Heat and Mass Transfer,* vol. 111, pp. 582–592, 2017.
[21] C.-K. Ma, P.-C. Tuan, J.-M. Chang, and D.-C. Lin, Adaptive weighting inverse method for the estimation of input loads, *International Journal of Systems Science*, vol. 34, no. 3, pp. 181–194, 2003.
[22] B. Bruscella, V. Rouillard, and M. Sek, Analysis of road surface profiles, *Journal of Transportation Engineering*, vol. 125, no. 1, pp. 55–59, 1999.
[23] J. M. Mendel, Lessons in estimation theory for signal processing, communications, and control. Pearson Education, 1995.
[24] P. S. Maybeck, Stochastic models, estimation, and control, *Academic press*, vol. 1, pp. 1-16, 1982.
[25] I. O. for Standardization, T. C. ISO/TC, M. Vibration, S. S. S. Measurement, E. of M. Vibration, and S. as A. to Machines, Mechanical Vibration–Road Surface Profiles–Reporting of Measured Data, vol. 8608. International Organization for Standardization, 1995.
[26] A. Gelb, Applied optimal estimation. MIT press, 1974.
[27] X. Zhang, M. Ba, J. Kang, and Q. Meng, Effect of soundscape dimensions on acoustic comfort in urban open public spaces, *Applied Acoustics*, vol. 133, pp. 73–81, 2018.
[28] T. Dao, T. Nguyen, J. Pan, Y. Qiao, and Q. Lai, Identification Failure Data for Cluster Heads Aggregation in WSN Based on Improving Classification of SVM, *IEEE Access,* vol. 8, pp. 61070–61084, 2020.
[29] T. Dao, J. Yu, T. Nguyen, and T. Ngo, A Hybrid Improved MVO and FNN for Identifying Collected Data Failure in Cluster Heads in WSN, *IEEE Access*, vol. 8, pp. 124311–124322, 2020.
[30] T.-T. Nguyen et al., A hybridized parallel bats algorithm for combinatorial problem of traveling salesman, *Journal of Intelligent and Fuzzy Systems*, vol. 38, no. 5, pp. 5811–5820, Feb. 2020.
[31] P. Wang, C.M. Chen, S. Kumari, M. Shojafar, R. Tafazolli, Y.N. Liu, HDMA: Hybrid D2D Message Authentication Scheme for 5G-Enabled VANETs, *IEEE Transactions on Intelligent Transportation Systems*, 2020, doi: 10.1109/TITS.2020.3013928.
[32] T. Y. Wu, Z. Y. Lee, L. Yang, J. N. Luo, R. L. Tso, Provably Secure Authentication Key Exchange Scheme Using Fog Nodes in Vehicular Ad-Hoc Networks, *Journal of Supercomputing*, 2021, https://doi.org/10.1007/s11227-020-03548-9
[33] C.M. Chen, B. Xiang, Y. Liu, K.H. Wang, A secure authentication protocol for Internet of vehicles, *IEEE Access*, vol. 7, pp. 12047-12057, 2019